Molecular insights into the self-assembly of hydrophobically modified chondroitin sulfate in aqueous media

Agata Żak [a], Grzegorz Łazarski [a], Magdalena Wytrwal-Sarna [b], Dorota Jamróz [a], Magdalena Górniewicz [a], Aleksander Foryś [c], Barbara Trzebicka [c], Mariusz Kepczynski [a,*]

[a] *Jagiellonian University, Faculty of Chemistry, Gronostajowa 2, 30-387 Kraków, Poland*
[b] *AGH University of Science and Technology, Academic Centre for Materials and Nanotechnology, A. Mickiewicza 30, 30-059 Krakow, Poland*
[c] *Centre of Polymer and Carbon Materials, Polish Academy of Sciences, Zabrze 41-819, Poland*

ARTICLE INFO

ABSTRACT

Hydrophobically modified chondroitin sulfate (CS) is widely used in the preparation of nano-sized drug delivery systems. Herein, the behavior of amphiphilic CSs in aqueous media and the drug accumulation inside the formed micelle-like structures were studied using experimental methods and molecular dynamics simulations. In particular, we focused on the impact of the degree of substitution (DS) with hydrophobic groups and the presence of drug on the morphology of the nanostructures and their molecular organization. Our results show that with increasing DS, the morphology of the amphiphilic CS nanostructures changes from irregular, loosely packed nanogels to cylindrical micelles with a core-shell architecture. These structures can efficiently accumulate hydrophobic drugs. However, the drug molecules preferentially locate at the interface between the hydrophobic part and the hydrophilic corona formed by the CS chains. Our work provides detailed information that may be relevant to the development of amphiphilic polysaccharide-based drug delivery systems.

1. Introduction

Polymeric nanoparticles are of great importance in the preparation of drug delivery systems (DDSs) (Amhare et al., 2020; Kowalczuk et al., 2014; Pippa et al., 2021). Polymer-based DDSs are used to improve various pharmacological and therapeutic properties of conventional ("free") drugs (for example, their pharmacokinetics and biodistribution) (Allen & Cullis, 2004), as well as for sustained drug release at the target site and minimizing toxicity by reducing off-site accumulation (Oommen et al., 2016). Due to their biocompatibility, non-immunogenicity, and biodegradability, biopolymers such as glycosaminoglycans (GAGs) are extensively studied to develop nanoscale DDSs for therapeutic purposes in the treatment of various diseases, including cancer, glaucoma, wounds, and burns (Misra et al., 2015; Yang et al., 2018). GAGs are a group of naturally occurring polysaccharides found in the extracellular matrix (ECM) of living organisms. This group includes compounds such as hyaluronic acid, heparin, and chondroitin sulfate (CS).

CS, an anionic polysaccharide found in the human body, is considered a preferred biomaterial for drug delivery and tissue engineering applications (Yang et al., 2020). In addition to its biocompatibility and biodegradability, CS is also hydrolyzed by microorganisms in the colon, consequently making it suitable for specific drug delivery to the colon (Cellet et al., 2015). In addition, this polysaccharide shows an affinity for the CD44 receptor, which is highly overexpressed in tumor cells, and therefore CS can be used to prepare tumor-targeted carriers (Li et al., 2021). Due to their high-water solubility, naturally occurring CSs are not

able to self-assemble into nanocarriers in aqueous environments. However, these hydrophilic polymers can be grafted with hydrophobic groups, thus obtaining amphiphilic polymers (Xie et al., 2021). When dispersed in an aqueous medium, the hydrophobically modified CSs spontaneously assemble into nanometric micelle-like structures with the CS chains on the outside and the hydrophobic groups forming the cores. The hydrophobic core can entrap water-insoluble drugs and release them in several ways (Zhao et al., 2015). In addition, the amphiphilic CS derivatives are biodegradable by enzymes (Misra et al., 2015). Therefore, amphiphilic CS-based nanostructures are good materials for specific drug delivery purposes. To modify CSs, oleic acid (Liang et al., 2020), α-tocopherol (Khan et al., 2020), deoxycholic acid (M. Liu et al., 2016, 2018), and linolenic acid (Xiao et al., 2014), among others, were attached as hydrophobic pendants. The obtained amphiphilic polymers were then used to prepare DDSs for several drugs. However, the micellization model of hydrophobically modified CSs or other GAGs and the spatial distribution of the drug inside the CS nanoparticles have never been evaluated in the literature. It is generally accepted that in aqueous media, such polymers form poorly defined structures with a wide size distribution (L. Li et al., 2014). It can be assumed that the behavior of amphiphilic CSs in aqueous media should strongly depend on their architecture. This leads to the hypothesis that the degree of substitution (DS) of CSs with hydrophobic groups and the incorporation of the hydrophobic drug affect the morphology and molecular organization of nanostructures formed by amphiphilic CSs in aqueous media.

In this work, a combination of experimental methods and atomistic-scale molecular dynamics (MD) simulations was used to investigate several aspects of the behavior of hydrophobically modified CS in the aqueous phase: (i) the effect of CS grafting with hydrophobic groups on the hydration of the polysaccharide backbone, (ii) the impact of DS on the aggregation ability of hydrophobically modified CS and morphology of the nanoparticles formed, and (iii) molecular organization of the nanoparticles. To this end, natural CS was converted into amphiphilic derivatives (CS-C18s) with different DS by covalent attachment of octadecyl groups. The ability of the amphiphilic derivatives to self-organize was investigated by determining the critical aggregation concentration (CAC) using fluorescence methods. Light scattering methods and cryo-transmission electron microscopy (cryo-TEM) were used to determine the size and morphology of the formed objects. A series of MD simulations were then performed to obtain a molecular view of the aggregate formation. Finally, we focused on the suitability of the obtained polymer structures as drug carriers. Curcumin was used as a model hydrophobic drug. Curcumin is a natural polyphenol that exhibits a wide range of desirable pharmacological properties, including anti-inflammatory, antioxidant, and neuroprotective effects (Karewicz et al., 2011).

2. Experimental section

2.1. Materials

Chondroitin sulfate A sodium salt from bovine trachea (product ID C9819, CS) was obtained from Sigma-Aldrich. This product was previously characterized: the weight-average molar mass (M_w) and number-average molar mass (M_n) were 30,700 Da and 22,100 Da respectively, the M_w/M_n ratio (molar mass dispersion) was 1.39, and the number of sulfate groups per disaccharide unit was 0.96 (Václavíková & Kvasnička, 2015). Octadecylamine (C18-NH$_2$) (≥99 %, GC), N-(3-dimethylamino-propyl)-N′-ethylcarbodiimide hydrochloride (EDC), N-hydroxysuccinimide (NHS, 98 %), tetrabutylammonium hydroxide (TBA, ~40 % solution in water, ~1.5 M), N-methylformamide (NMF), 1,6-diphenyl-1,3,5-hexatriene (DPH), curcumin (Cur, curcuminoid content ≥94 %, Cur content ≥80 %), phosphate-buffered saline (PBS, tablets), dialysis tubes (high retention seamless cellulose tubing, molecular weight cutoff 14,200 g/mol), Dowex 50 W X8 ion-exchange resin (hydrogen form, 200–400 mesh), DMSO-d_6 (99.9 atom % D), and D$_2$O (99.9 atom % D)

were purchased from Sigma-Aldrich. N,N-dimethylformamide (DMF) and tert-butanol were obtained from Chempur. Millipore-quality water was used in all experiments.

2.2. Synthesis of CS-C18s

Three CS derivatives (CS-C18s) differing in the degree of substitution (DS) with octadecyl groups were obtained. The structure of CS-C18s is shown in Fig. 1A. Derivatives with lower DS were obtained according to the modified procedure described previously (Szafraniec et al., 2017). Briefly, CS (100 mg) was dissolved in deionized water (20 mL). EDC (8.0 mg, 41.2 μmol or 19.8 mg, 103.0 μmol) was added and the solution was stirred for 1 h. NHS (4.48 mg, 41.2 μmol or 12.1 mg, 103.0 μmol) was then added, and stirring was continued for 2 h. C18-NH$_2$ (12.2 mg, 41.2 μmol or 28.0 mg, 103.0 μmol) was dissolved in a mixture of DMF and chloroform (20 mL, 4:1). This mixture was added to the aqueous solution of CS and vigorously stirred for 48 h at 37°C. The suspension was dialyzed against a 1:1 (v/v) mixture of tert-butanol and PBS for 3 days, then against deionized water for 4 days. The product was isolated by lyophilization. 95 mg of CS-C18_1.5 (93 % yield) and 102 mg of CS-C18_6.5 (90 % yield) were obtained. For the higher DS, the procedure previously described was used (Cadete et al., 2019). Briefly, CS was converted to the tetrabutylammonium salt. The salt was dissolved in a DMF/NMF mixture (50 mL, 4:1), EDC (186.24 mg) and NHS (111.55 mg) were added, and the mixture was stirred for 2 h. C18-NH$_2$ (261.4 mg dissolved in 2 mL of DMF) was added and the mixture was stirred for 48 h at 37 °C. The dispersion was then dialyzed against 0.1 M NaCl/tert-butanol mixtures with decreasing tert-butanol content: 1:1, 2:1, 3:1, 5:1 and 9:1, and finally against deionized water for three days. The product (CS-C18_33) was isolated by lyophilization (0.42 g, 95 % yield) The degrees of substitution with alkyl groups were estimated by NMR analysis (**Fig. S1**). DS was determined from the ratio of the peak area of the methyl protons of the CS acetamide group (at δ = 2.0 ppm) and the terminal methyl protons of the octadecyl substituent (at δ = 0.87 ppm) (Szafraniec et al., 2017). The results are shown in Table 1.

2.3. Preparation of aggregates

To prepare CS-C18 dispersions, the polymers with lower DS were dispersed directly in PBS (1 mg/mL) and stirred overnight. In the case of CS-C18_33, the polymer was dispersed in a THF/PBS mixture (1:1.5 v/v), then PBS was added dropwise, and the mixture was stirred overnight to evaporate the organic solvent. The final polymer concentration was 1 mg/mL. For Cur-loaded structures, an appropriate volume of a drug solution in ethanol (3 mg/mL) was added to the CS-C18_33 dispersion in the THF/PBS mixture to achieve the intended Cur content (10, 15, or 20 wt% relative to the polymer). The CS-C18 dispersions were then diluted to the desired concentration. The samples were shortly sonicated (amplitude: 20 %, pulser: 2 s–2 s, time: 1–5 min) using a 500 W ultrasonic processor (VCX 500, Sonics & Materials, USA).

2.4. Dynamic light scattering (DLS)

DLS and ζ-potential measurements were performed using a Malvern Nano ZS light-scattering apparatus (Malvern Instrument Ltd.) as described previously (Kepczyński et al., 2006). The time-dependent photocurrent autocorrelation function was recorded every 10 s performing 15 acquisitions for each run at 22 °C. The z-averaged hydrodynamic mean diameter (dz), polydispersity index (PDI), and distribution profile of each sample were calculated using the software provided by the manufacturer.

2.5. Fluorescence measurements

The fluorescent molecular probe method was used to determine the critical aggregation concentrations (CACs) (Chattopadhyay & London,
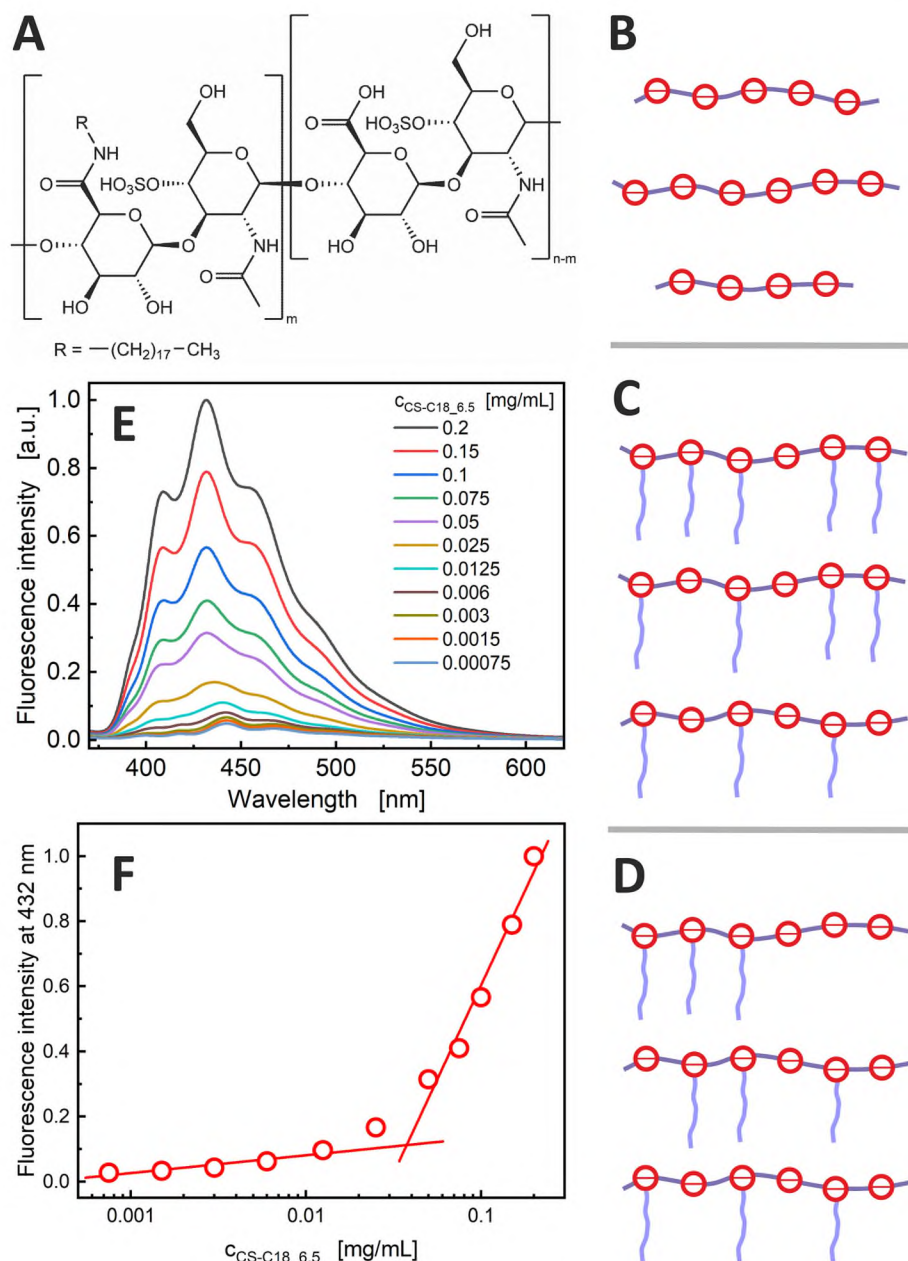
Fig. 1. (A) Chemical structure of CS-C18s. (B,C,D) Schematic representation of the polydispersity of polyelectrolytes, the difference in the degree of substitution of individual polymer chains, and the different distribution of the hydrophobic groups along the polymer backbone. (E) Fluorescence spectra of DPH (4 μM, λex = 350 nm) in the presence of CS-C18_6.5 at increasing concentrations. (F) The fluorescence intensity of DPH at 432 nm as a function of the CS-C18_6.5 concentration.

1984). A stock solution of DPH (0.4 mM) was prepared in methanol by short sonication in an ultrasonic bath. A series of samples containing DPH at a constant concentration (4 μM) and the polymer at concentrations ranging from 0 to 0.2 mg/mL were prepared and stirred for 2 h in the dark. The fluorescence spectra of these samples (excitation at 350 nm) were measured using a Hitachi F-7000 fluorescence spectrophotometer.

2.6. Cryogenic transmission electron microscopy (cryo-TEM)

The morphology of objects suspended in water was observed using a Tecnai F20 X TWIN microscope (FEI Company, Hillsboro, Oregon, USA) equipped with a field emission gun operating at a 200 kV acceleration voltage and a Gatan Rio 16 CMOS 4 k camera (Gatan Inc., Pleasanton, California, USA). Details of the sample preparation and measurements were previously described (Zatorska-Plachta et al., 2021).

3. Molecular dynamics simulations

3.1. System preparation

CS and CS-C18 were modeled by oligomers composed of 23 disaccharide units. In the case of CS-C18, the polysaccharide chain was substituted with octadecyl groups attached via an amide bond (Fig. 2A), with degrees of substitution of about 10 %, 25 %, 40 %, and 100 % (CS-C18$_{10}$, CS-C18$_{25}$, CS-C18$_{40}$, and CS-C18$_{100}$ oligomers, respectively). We simulated systems (Table 2) containing: (1) a single oligomer (systems **E** and **F**), (2) four oligomers (systems **A**, **B**, **C**, and **D**), and (3) four oligomers and 18 Cur molecules (systems **G**), placed in a simulation box with water. The negative charge of CS was neutralized by introducing K$^+$ counterions, then K$^+$ and Cl$^-$ ions were added so that the ionic strength was 0.14 M (a value similar to that used in the experiment). The systems were subjected to energy minimization, followed by equilibration, and

Table 1

Degree of substitution (DS) of CS with octadecyl groups and values of the critical aggregation concentration (CAC). Values of the mean hydrodynamic diameter (dz), size dispersity expressed as an index of polydispersity (PDI) and zeta potential (ζ) of CS-C18 nanostructures dispersed in PBS at a concentration of 0.4 mg/mL.[a]

System	DS	CAC (μg/mL)	dz (nm)	PDI	ζ (mV)
CS-C18_1.5	~1.5 %	49 ± 3	360 ± 12	0.32 ± 0.05	−37.7 ± 1.0
CS-C18_6.5	~6.5 %	39 ± 4	348 ± 10	0.24 ± 0.02	−35.1 ± 1.0
CS-C18_33	~33 %	17 ± 2	253 ± 9	0.36 ± 0.01	−27.3 ± 0.7
CS-C18_33 + 10 % Cur	~33 %	–	445 ± 13	0.35 ± 0.04	−27.1 ± 1.6

[a] Values are the mean ± standard deviation, n = 5.

finally production simulations.

3.2. Force field parameters and simulation details

All molecules were described using CHARMM36 parameters. The basic unit of CS was modeled with the CHARMM-GUI utility (Jo et al., 2008; Lee et al., 2016) using the Glycan Modeler module (Park et al., 2019), then it was replicated using a custom-made software to give an oligomer of the desired length. The parameterization of Cur was described previously (Kepczynski & Jamróz, 2020). The enolic tautomeric form of Cur was simulated, according to the experimentally determined relative abundance of various tautomers (Anjomshoa et al., 2016). Water was represented by the CHARMM compatible TIP(S)3P model (Jorgensen et al., 1998). All simulations were performed with the GROMACS 2019 simulation software (Abraham et al., 2015; Pronk et al., 2013; van der Spoel et al., 2005). Temperature was controlled by the "V-rescale" thermostat. The pressure was controlled at 1 bar using the isotropic Parrinello-Rahman barostat (Parrinello & Rahman, 1998) (τ = 2 ps). All hydrogen-containing bonds were constrained using LINCS (Hess et al., 1997). Van der Waals interactions and short-range repulsion were described by a Lennard-Jones potential with a cut-off of 1.2 nm. Electrostatic interactions were calculated using the particle-mesh Ewald (PME) method (Darden et al., 1998) using a 1.2 nm real-space cut-off and 0.16 nm Fourier grid. The dispersion correction 'EnerPress' was applied. Equilibration of the system was performed for 100 ps in an NVT ensemble, followed by another 100 ps in an NpT ensemble. The analysis of trajectories was performed using the tools included in the GROMACS package and the VMD package. (Humphrey et al., 1996). All snapshots were prepared using VMD. Plots for the MD portion were prepared with Matplotlib (Hunter, 2007).

4. Results and discussion

4.1. Grafting polyelectrolytes with hydrophobic groups results in substantially non-uniform materials

Three hydrophobically modified CS derivatives differing in DS were obtained by grafting the polysaccharide chain with the octadecyl moieties (Table 1). Generally, hydrophobically grafted polyelectrolytes should be considered polydisperse and non-homogeneous materials due to several factors: (i) polymers are not monodisperse and consist of polymer chains of different length (Fig. 1B). The molar mass dispersity of the CS used in these studies was approximately 1.4. (ii) CS chains can be substituted with a different number of octadecyl groups due to the random course of the substitution reaction. This means that polymer chains can differ in the DS values (Fig. 1C), and the determined value of the degree of substitution is only an average for all chains. (iii) The distribution of the hydrophobic groups along the polymer backbone may

vary for each polysaccharide chain (Fig. 1D). In other words, within one polymer chain there can be fragments with higher DS and fragments with lower DS, which is also associated with the random course of the substitution reaction. The dispersity and heterogeneity of amphiphilic polyelectrolytes should influence their physical properties and behavior in aqueous solutions.

4.2. CS-C18s aggregate in aqueous media with the formation of hydrophobic domains

Hydrophobically modified polymers can spontaneously form micelle-like structures above the critical aggregation concentration (CAC) (Liu et al., 2010; Wytrwal et al., 2011). Fluorescence measurements using DPH as a molecular probe were used to study the aggregation of CS-C18s in an aqueous environment. For this purpose, a series of samples containing a constant DPH concentration and various mass fractions of the polysaccharides were prepared, and fluorescence spectra of DPH were measured (Fig. 1E). DPH showed weak emission in the water phase and its fluorescence intensity increased with increasing polymer concentration in the system, which is related to the transition of the fluorophore molecules to the hydrophobic domains formed by the alkyl groups of the CS-C18s. The CAC value for CS-C18s was determined from the dependence of the fluorescence intensity on the polymer content as the intersection of two lines fitted to the two regions defined for low polymer concentrations and when the DPH fluorescence intensity increased sharply (Fig. 1F). The CACs are shown in Table 1. As expected, the CAC values dropped significantly as DS increased. A similar dependence was observed for CS modified with other hydrophobic groups. The CAC values for α-tocopherol-substituted CS decreased from 0.040 mg/mL to 0.027 mg/mL, as the DS increased from 2.5 % to 4.6 % (Li et al., 2021). In turn, the CS substituted at 2.5 % and 7 % with deoxycholic acid were characterized by the CAC values of 0.05 and 0.027 mg/mL, respectively (Xie et al., 2021). Both our results and the values reported in the literature show that amphiphilic CS derivatives aggregate already at concentrations of several dozen μg/mL.

The size of objects formed in the CS-C18 dispersions at concentrations above CAC was determined using the light scattering measurements (Table 1). As DS increased, the size of the aggregates decreased, probably due to increased attraction between the octadecyl groups, which tend to avoid contact with water. As a result, aggregates formed by the polymers with higher substitution of alkyl groups should have a more compact structure. Another explanation could be the effect of the degree of CS substitution on the number of macromolecules forming the aggregate. For low DS, a larger number of polysaccharide chains may form aggregates, thus increasing their size.

The zeta potential is an important parameter for predicting the stability of dispersion systems. It is assumed that absolute values of ζ-potential >30 mV provide long-term stability of aqueous dispersions (Lewandowska et al., 2009). The CS-C18 particles were characterized by relatively high negative ζ-potentials (Table 1). This high negative charge is due to the presence of ionized carboxyl groups and sulfate groups. However, the potential values increased with increasing DS, which is likely related to the conversion of negatively charged carboxyl groups to neutral amide groups. A similar trend was observed previously for CS derivatives with linoleic moieties, for which the ζ-potential increased from −36 mV to −25.4 mV, while the DS increased from 0.034 % to 0.123 % (Liang et al., 2020). On the contrary, the opposite trend was observed for α-tocopherol and deoxycholic-substituted CSs, but no explanation was provided (Khan et al., 2020; Liang et al., 2020).

4.3. Cryo-TEM reveals the formation of irregular nanogels and cylindrical micelles depending on the degree of polysaccharide substitution with octadecyl groups

The morphology of aggregates formed by the CS-C18s above the CAC was visualized by cryo-TEM microscopy. Fig. 3 shows cryo-TEM
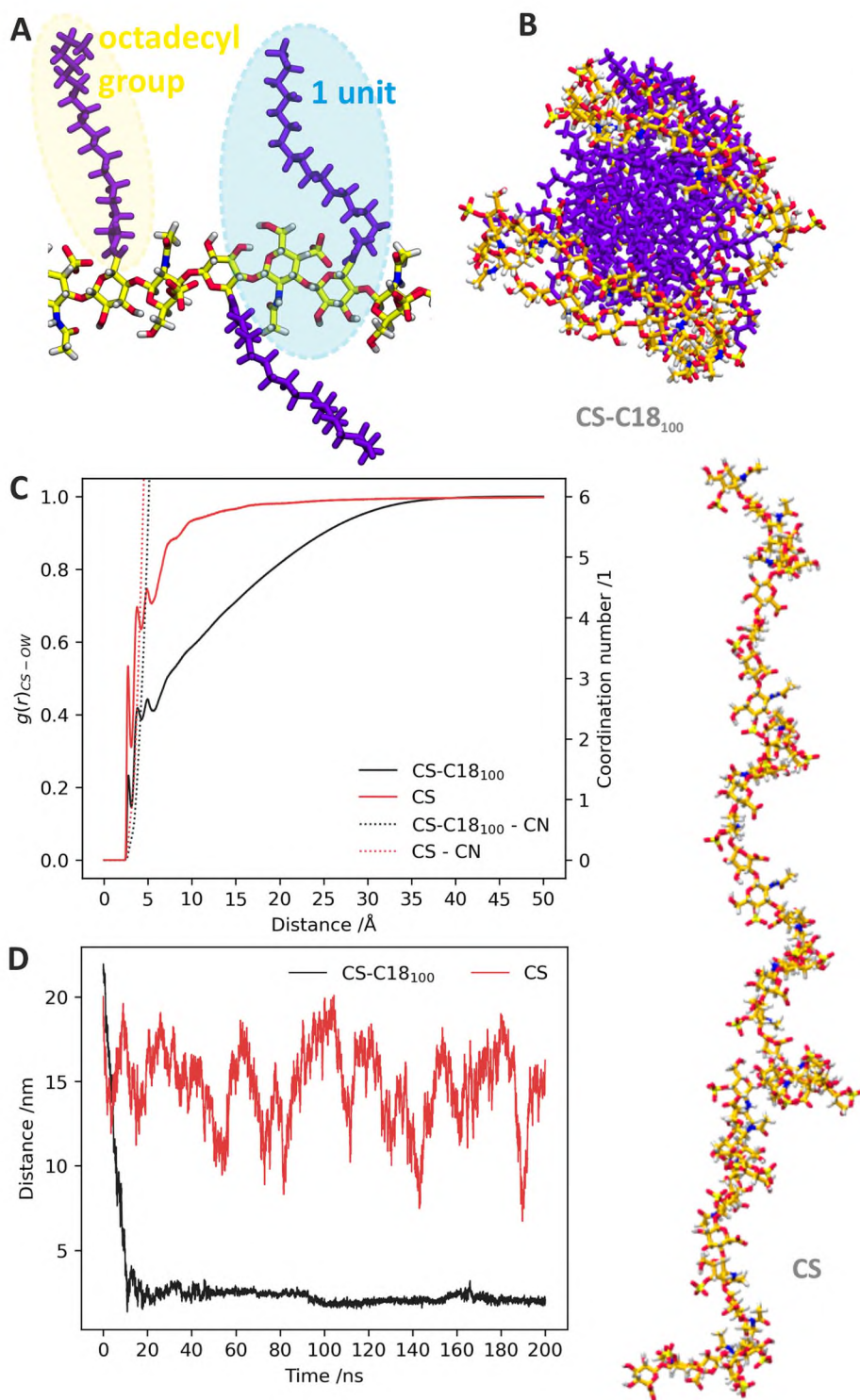
Fig. 2. (A) A fragment of CS-C18$_{100}$ oligomer used in the MD simulations. Octadecyl groups are shown in purple. Oxygen and nitrogen atoms are shown in red and blue, respectively. (B) Snapshots of systems taken at $t = 100$ ns of MD simulations. (C) The g$_{CS-OW}$(r) radial distribution functions (RDFs) for the atomic pairs of CS oligomer − water oxygen (OW) and CS-C18 oligomer − water oxygen (OW). The functions were averaged over the last 75 ns of the simulation. (D) Time development of the end-to-end distance for the CS (red) and CS-C18 (black) oligomers calculated from the simulations.

micrographs of the hydrophobically modified CS dispersions. For CS-C18_1.5, two types of particles were observed: irregular objects with low contrast and sizes in the range of 15–150 nm, and rod-like particles with a sharp contrast, 10–90 nm in length, and 6–9 nm in diameter (Fig. 3A). Images of the CS-C18_6.5 dispersion also reveal the presence of at least two populations of objects: a more numerous population of rod-like particles, which are 10–90 nm in length and 6–9 nm in diameter, and sparse irregular low-contrast objects with a size of 15–80 nm (Fig. 3B). The rod-like structures indicate the formation of cylindrical micelles in the system. While the low-contrast particles are loosely

packed strongly hydrated nanogels. In aqueous dispersions of CS-C18_33 prepared at a concentration above the CAC, microscopic analysis revealed the presence of high-contrast rods. The length of these cylindrical micelles varied in the range of 20–410 nm, and their diameter was between 6 and 20 nm (Fig. 3C). A different picture was observed for the dispersion prepared by dissolving CS-C18_33 at a concentration below the CAC and then concentrating the solution above the CAC (Fig. 3D). Mainly, a large number of small nanoparticles with a size of 2–3 nm are observed, which organize into larger clusters of irregular shape. These structures can be attributed to the formation of globular polymer

Table 2
Summary of the simulated systems.[a] All simulations were performed at 298 K and ionic strength of 0.14 M.

System	Oligomer type	Oligomers (N)	Cur	Water molecules	Simulation time [ns]
A	$CS\text{-}C18_{10}$	4	–	391,712	2×220
B1	$CS\text{-}C18_{100}$	4	–	451,250	200
B2	$CS\text{-}C18_{100}$	4	–	491,565	2×200
C	$CS\text{-}C18_{25}$	4	–	495,808	200
D	$CS\text{-}C18_{40}$	4	–	495,559	200
E	$CS\text{-}C18_{100}$	1	–	489,640	2×200
F	CS	1	–	427,829	2×200
G	$CS\text{-}C18_{100}$	4	18	389,682	200

[a] The table indicates the number of oligomers in the system (N) and Cur molecules in each system, the number of repetitions for equilibrium simulations and the corresponding simulation times.

micelles. When the CS-C18_33 concentration was lower than the CAC, the single polymer coiled up to form monomolecular micelles. As a result of the dispersion concentration, these micelles combined into larger structures. The high-contrast cylindrical micelles were also formed in this case (Fig. 3D), but their sizes were smaller than those prepared for concentrations that were initially larger than the CAC. The discrepancy between the sizes of structures determined by cryo-TEM and DLS is probably related to the fact that the intensity of scattered light increases strongly with increasing object size. Therefore, the DLS method is significantly biased towards the largest objects (e.g., particle aggregates) and thus particle sizes obtained with DLS may be overestimated.

The molar mass dispersity and substitution heterogeneity of the hydrophobically modified CSs result in the formation of structures of various morphologies and sizes. In polymer dispersions, we always deal with aggregates composed of polymer chains of different lengths, which results in a distribution of sizes of the observed objects. However, the existence of structures with different morphologies (nanogels and cylindrical micelles) in equilibrium can be explained by assuming segregation in the aggregation of polymer chains due to their different substitution with hydrophobic groups. This led us to hypothesize a previously unforeseen mechanism: in a given system, polymer chains with less alkyl substitution form loosely packed structures, while the more hydrophobically substituted chains self-assemble separately to form more compact (high contrast) cylindrical micelles. This mechanism is also supported by the fact that the share of nanogel structures decreases for derivatives with higher substitution, while the number of densely packed rods formed by chains with higher DS increases.

The morphology of nanoparticles formed by hydrophobically modified CSs has been previously investigated using conventional TEM and spherical shaped nanoparticles were generally observed. For example, for α-tocopherol derivatives of CS, spherical nanoparticles with a diameter of ~140 nm were observed by TEM microscopy (M. Li et al., 2021). The smooth sphere morphology and a uniform size distribution of micelles formed by CS substituted with α-linolenic acid were reported (Liang et al., 2020). TEM microscopy also revealed the spherical morphology of nanoparticles obtained from deoxycholic-substituted CS (Xie et al., 2021). However, conventional TEM requires the sample to be dried prior to measurement, therefore the observed morphologies are for particles in the dried state. The process of sample dehydration undoubtedly significantly affects the morphology of structures obtained from highly hydrated polymers such as CS. The use of cryo-TEM microscopy, in which the sample is not subjected to any preparation processes, allows the objects to be observed in the hydrated, and therefore undisturbed, state.

4.4. MD simulations showed that the attachment of alkyl chains has a moderate effect on the hydration of CS chains

The tendency of polymers to aggregate in an aqueous environment is

strongly related to their hydration. Therefore, we first used MD simulations to examine the degree of hydration of CS-C18s and compared it to that of the parent polymer. For this purpose, a single $CS\text{-}C18_{100}$ or CS (systems E and F, respectively) oligomer placed in a water-filled box was simulated. The final configurations of the CS and $CS\text{-}C18_{100}$ oligomers are shown in Fig. 2B. CS has several groups that can interact with water molecules: sulfate, carboxyl, acetamide, and three hydroxyl groups that are evenly distributed around the two pyranose rings (see Fig. 1). To analyze the static associations of water molecules and counterions with CS chains, we calculated radial distribution functions (RDFs) for the polar groups of CS and water molecules, and potassium cations. The RDF functions for the CS oligomer − water oxygen (OW) pairs and for the $CS\text{-}C18_{100}$ oligomer − water oxygen (OW) pairs are shown in Fig. 2C. The RDF functions were normalized by the density for the whole simulation box, which allowed us to obtain the number of counterions and water molecules in different solvation shells. A cartoon representation of the polar interaction network is shown in Fig. 4. The results indicate that CS is highly hydrated in an aqueous solution. Each disaccharide repeating unit is associated with about 32 water molecules in the first hydration shell. The potassium cations are located near the polymer chain, but a negligible amount is in direct contact with the negatively charged CS groups (sulfate and carboxyl). Fig. 2B shows that despite the strong hydration and repulsion between the negatively charged groups located along the polysaccharide backbone, the CS chains retain highly flexible and are not fully stretched. They can freely change their conformations, as evidenced by the large variability of the end-to-end distance during the simulations (Fig. 2D). A distribution of the end-to-end distances for the CS oligomers, shown in Fig. 4c, is broad with an average value of 14.8 nm. All this indicates that the chains of unsubstituted chondroitin sulfate have a great conformational freedom in aqueous media. In turn, the presence of octadecyl moieties forced the polysaccharide chain to coil into a compact structure with the alkyl groups located in the center (Fig. 2B). The entire process was fast and after 20 ns, the CS-C18 globule gained a stable structure that did not change until the end of the simulation, as evidenced by the low variation in the end-to-end distance (Fig. 2D). The distance distribution between the ends of the CS-C18 oligomer chains is very narrow compared to the values for CS, and the average end-to-end distance value is about 2.5 nm (Fig. 4c). This clearly indicates that the hydrophobically modified CSs with high DS adopt a very compact stable conformation, forming monomolecular micelles even at low concentrations. The calculated RDFs revealed that the attachment of alkyl groups decreased the hydration of the CS chains. About 23 water molecules are bound to each octadecyl-substituted disaccharide repeating unit in the first hydration shell (Fig. 4). This indicates that the polysaccharide backbone in the CS-C18s remains highly hydrated.

It is well known that CSs possess excellent hydrophilicity and the high hydrodynamic volume while circulating in the body that can inhibit undesirable interactions with plasma proteins and cells (Park et al., 2010). Hydration of CS has been studied previously both experimentally and using MD simulations. An infrared spectroscopic study showed that 3.1 ± 0.2 water molecules are specifically bound to one CS repeating unit (Servaty et al., 2001). Using short MD simulations, the number of hydrogen bonds between the water molecules and the acceptor atoms of chondroitin 4-sulfate was determined to be about 20 per disaccharide unit (Kaufmann et al., 1999).

4.5. MD simulations show on a molecular scale how the degree of substitution of hydrophobically modified CSs affects their aggregation

Next, to understand the formation mechanism and the molecular organization of CS-C18 aggregates, MD simulations of five systems containing four oligomers with different DS placed in an aqueous medium were performed (systems **A**, **B**, **C**, and **D**, Table 2). In all of these systems, the concentration of oligomers was >1 mg/mL, thus significantly exceeding the CAC values measured for the real polymers
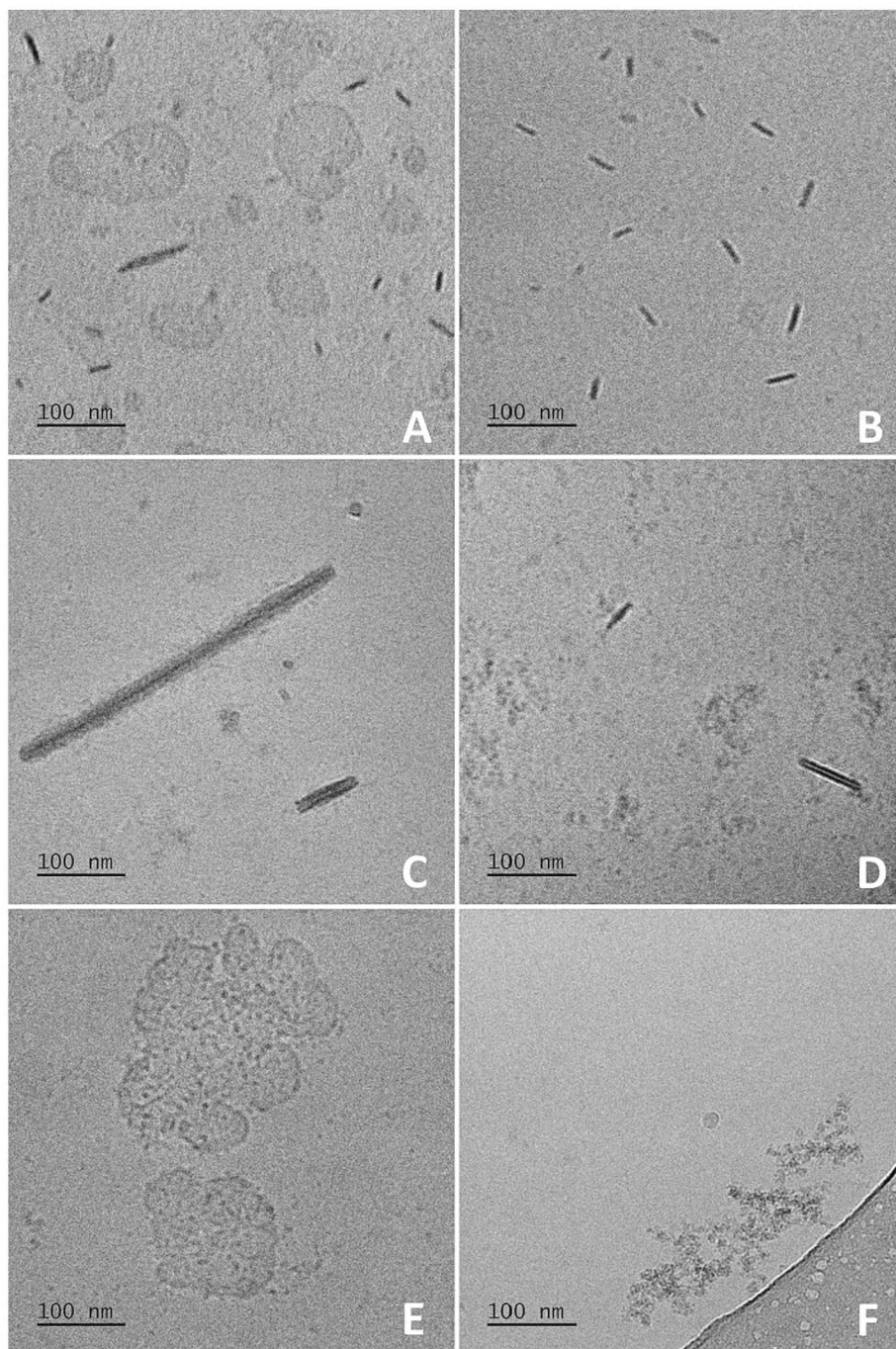
Fig. 3. Cryo-TEM micrographs of structures formed in aqueous dispersions of CS-C18_1.5 (A), CS-C18_6.5 (B), and CS-C18_33 (C) at concentrations above the CAC. (D) Cryo-TEM micrograph of CS-C18_33 structures prepared at a concentration below CAC and then concentrated to a concentration above CAC. (E,F) Cryo-TEM micrographs of CS-C18_33 structures (0.4 mg/mL) with embedded Cur (20 wt%).

(Table 1). Snapshots showing the final configurations of the calculated systems are shown in Fig. 5. Since, the polysaccharide chains are highly hydrated, interactions between hydrophobic groups attached to CS are basically responsible for aggregation. Therefore, to quantify the interactions between oligomers and their ability to assemble, the numbers of intermolecular (i.e., between alkyl groups attached to different CS chains, N_{inter}) and intramolecular (between alkyl groups attached to the same CS chain, N_{intra}) contacts between the atoms of octadecyl groups were calculated. The contact was assumed to occur when the distance between the octadecyl atoms was <0.46 nm. The number of intermolecular and intramolecular contacts averaged over the last 120 ns is listened in Table S1. To assess the conformation of the polysaccharide chains (elongated or coiled), the end-to-end distances averaged over the last 120 ns for the four oligomers were calculated for each system (Fig. 4c).

In the case of CS-C18$_{10}$ (systems A), the polysaccharide chains are elongated and can change their conformations relatively freely, as indicated by the broad distribution of the end-to-end distances (Fig. 4c). With little substitution, the hydrophobic groups are far apart, making their intramolecular contacts difficult (**Table S1**). The strong repulsion between the negatively charged groups on the CS backbone causes the oligomers to be far apart. However, single contacts between the octadecyl groups attached to different oligomers were observed during the simulation (**Table S1**). Thus, it can be assumed that at very low DS,
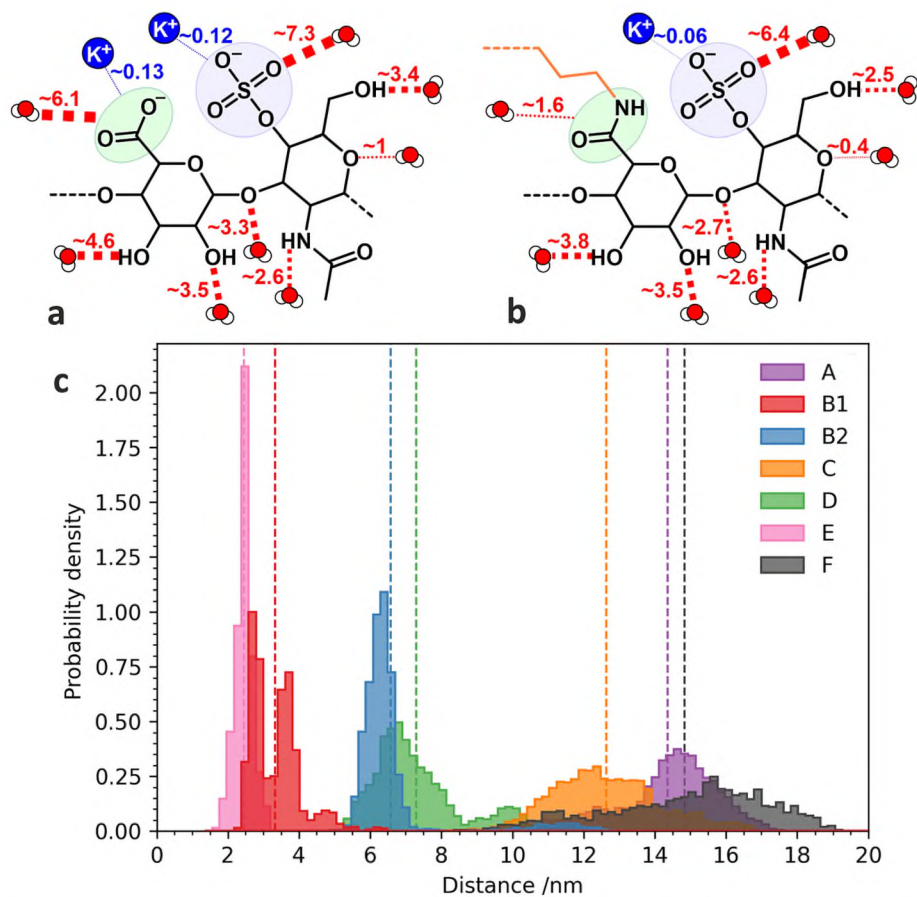
Fig. 4. Cartoon representations of all possible hydrogen bonds (red dashed lines) and charge pairs (blue dashed lines) for CS (a) and CS-C18$_{100}$ (b). (c) Distributions of the end-to-end distances of the CS-C18 oligomers (see Table 2) calculated from the simulations. The average value is indicated by vertical lines.
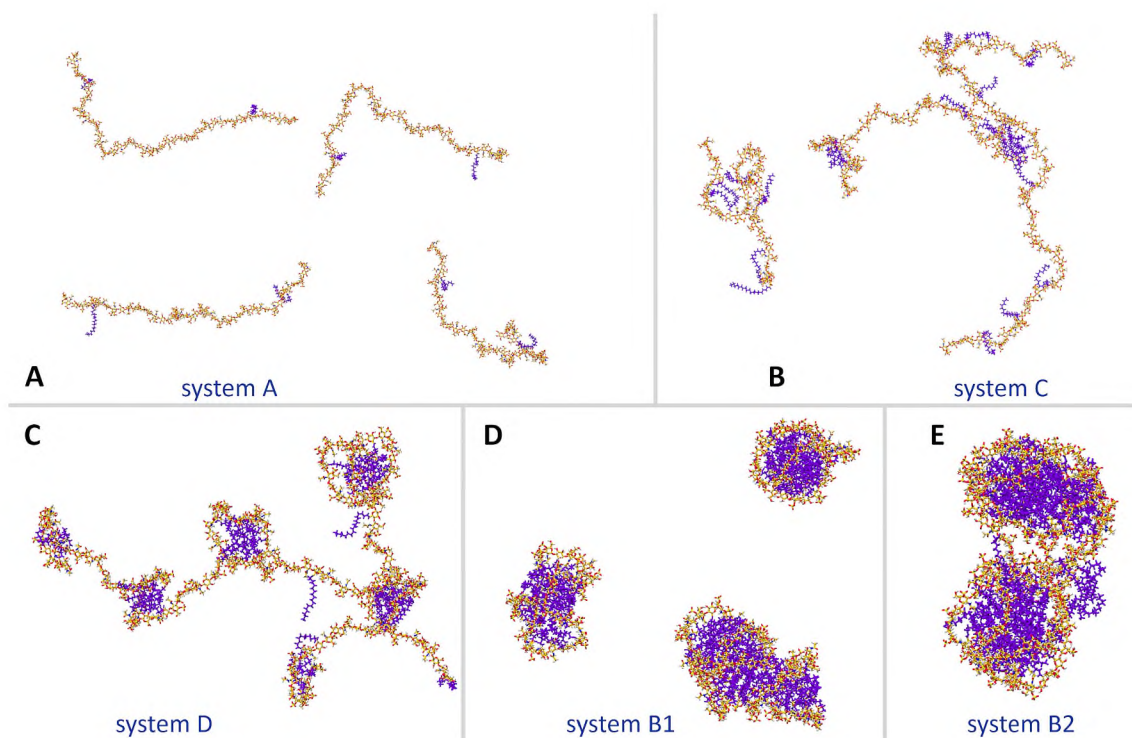

Fig. 5. Snapshots of simulated systems containing 4 CS-C18 oligomers with different DS at the end of the simulations. The oligomers are depicted as licorice and colored according to atom type. The octadecyl groups are shown as purple sticks. For clarity, water and ions are not depicted.

loosely packed, highly hydrated aggregates are formed as a result of intermolecular interactions between octadecyl groups. The number of intermolecular and intramolecular contacts increased as the DS increased to 25 % (system **C, Table S1**). Although the CS-C18$_{25}$ chains remained elongated and retained some conformational freedom (Fig. 4c), the intermolecular contacts between the alkyl groups allowed aggregation of the oligomers, while the intramolecular contacts resulted in the formation of small hydrophobic domains. For CS-C18$_{40}$ (system **D**), a significant increase in intramolecular interactions was observed (**Table S1**). The octadecyl groups formed several hydrophobic cores (Fig. 5C), which caused the polysaccharide backbones to fold, but the whole structure remained loosely packed and highly hydrated. This is consistent with the formation of nanogels that have been observed experimentally. In the case of CS-C18$_{100}$ (systems **B**), the final structures strongly depend on the initial configuration of the simulated system. When the oligomers were initially spaced apart (system **B1, Fig. S3**), two polysaccharide chains folded strongly to form monomolecular micelles (Fig. 4c). The remaining two oligomers aggregated during the simulation with the formation of an elongated small micelle. In both cases, the alkyl groups formed densely packed hydrophobic cores, and the CS backbones were exposed to the water phase. The formation of monomolecular micelles is likely related to the slow diffusion of polysaccharide chains in the aqueous environment and strong intramolecular interactions (**Table S1**). Thus, the MD results support the possibility of the formation of monomolecular micelles in the CS-C18_33 dispersion at concentrations below the CAC, as observed in cryo-TEM. In contrast, the simulation of system **B2**, in which the oligomers were initially in close contact (**Fig. S3**), led to the formation of cylindrical micelles (Fig. 5E). The N_{inter} value in this system was much higher than N_{intra}, showing that the oligomers building the micelle are strongly associated with each other. Such cylindrical micelles were also observed experimentally for the dispersion of the polymers with high DS at concentrations above the CACs. In both **B** systems, the end-to-end distance distributions were very narrow and the number of total contacts between alkyl groups was the same. This shows that the polysaccharide chains had a very limited ability to change conformation, thus the micelles had a very rigid structure.

To explore the internal structure of the aggregate formed by the most substituted oligomers, density maps in three planes perpendicular to the principal rotation axes of the globule were calculated (Fig. 6A). The maps reveal that the alkyl groups form densely packed cores that contain no water molecules, and one cylindrical micelle can consist of several such cores (multi-core micelle) (Fig. 6). The main CS chains are highly hydrated and are located on the surface of the micelle. The simulations (system **B1**) indicate that, in the case of CS derivatives with a high DS, monomolecular micelles with highly corrugated polysaccharide chains can also be formed. These images are consistent with microscopic observations. Indeed, small globular particles and rod-like particles were observed for polymers with higher degrees of grafting with alkyl groups.

The direct comparison of the experimental results and the MD simulations requires great care due to the limitations and simplifications of the simulations. The first limitation is related to the size of the systems and the length of the simulations. In the calculations, we used oligomers that were evenly substituted with alkyl groups along the polysaccharide chain. While in the real system, the polymers were several times longer, and their substitution was rather uneven. Thus, the simulated oligomers can be viewed as fragments of the real polymer with different DS. The second limitation arises from overestimating electrostatic interactions in MD simulations (King et al., 2021), which significantly increases the repulsive forces between negatively charged CS chains, and thus may hinder the polymer aggregation process. Keeping these limitations in mind, the MD simulations can provide some insight into the molecular picture of the self-assembly of hydrophobically modified CSs.

Our simulations show that the morphology of the aggregates formed depends very strongly on the degree of CS substitution with C18 groups and the polymer concentration, which in turn affect the intermolecular and intramolecular interactions between alkyl groups. At very low DS, polysaccharide chains adopt elongated conformations that can freely change over time. The low density of hydrophobic groups along the CS chain results in negligible intramolecular interactions, so such derivatives can aggregate due to dimer formation between alkyl groups attached to different chains. This results in poorly defined, loosely packed structures with a wide size distribution, giving low contrast in cryo-TEM due to strong hydration (but should be visible in conventional TEM microscopy after sample drying). Increasing the number of hydrophobic substituents increases the possibility of intramolecular interactions, leading to the formation of small hydrophobic domains that can accumulate non-polar substances. The fluorescence measurements showed that such domains can be formed at DS = 1.5 %. The polysaccharide chains become more coiled and the whole structure is better
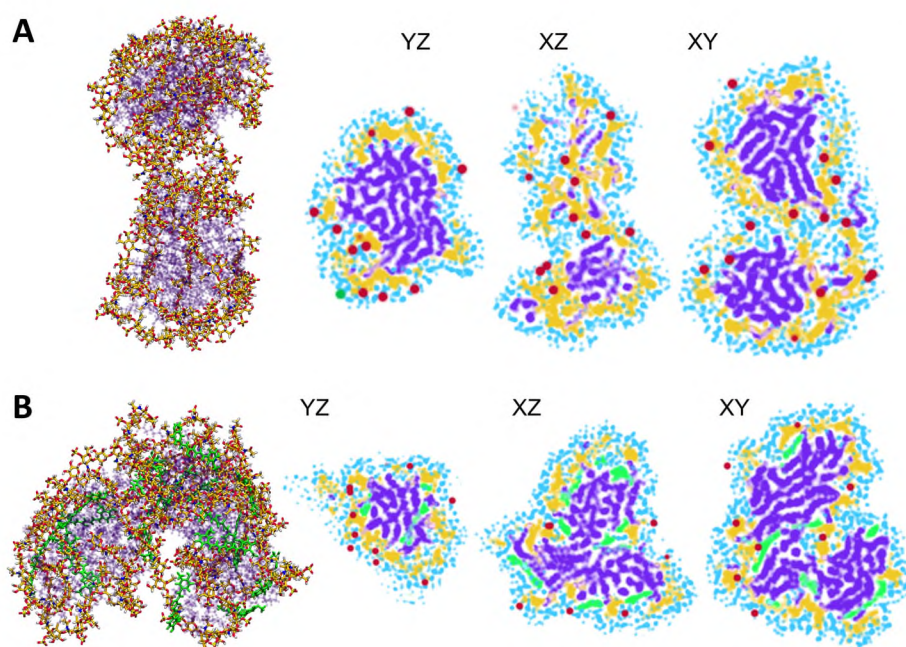

Fig. 6. Snapshots of the configurations of the **B2** (A) and **G** (B) systems (Table 1) at $t = 200$ ns. Oligomers are colored according to atom type. The hydrophobic side chains were colored purple and made transparent. Cur molecules are depicted in green. For clarity, water and ions are not depicted. The corresponding two-dimensional density maps computed in three planes intersecting the polymer coils for both systems are shown on the right. Hydrophobic domains (purple) were surrounded by CS chains (orange). Also shown are water molecules (cyan) and K$^+$ (crimson) located <0.5 nm from the polymer coil. Cur molecules are depicted in green.

defined, forming nanogels, visible by cryo-TEM. The size of the hydrophobic domains should increase with increasing DS. Further increasing the density of alkyl groups along the chain enhances intramolecular interactions, which promotes the formation of hydrophobic cores (Fig. 5C). Beyond a certain content of alkyl groups, well-defined densely packed structures are formed whose morphology depends on the polymer concentration. At concentrations below CAC, monomolecular aggregates and small micelles may form as a result of intramolecular contacts, which may assemble into larger clusters as a result of intermolecular interactions between alkyl groups (Fig. 5D). In contrast, above the CAC concentration, dispersions of hydrophobically modified polysaccharides should be dominated by multicore micelles in which the structure is maintained primarily by intermolecular contacts between hydrophobic groups (Fig. 5E). Computational modeling of CS-C18 aggregation confirmed that cylindrical micelles can be formed for highly substituted polysaccharides.

4.6. Nanoparticles obtained from CS-C18 with high DS can efficiently accumulate hydrophobic drugs

The presence of hydrophobic drugs can lead to changes in the aggregation process of amphiphilic polysaccharides. Therefore, we measured the CAC value for CS-C18_33 in the presence Cur. Fluorescence measurements using Cur as a molecular probe were performed. Fluorescence spectra of the drug were measured for a series of samples containing a constant Cur concentration (41 μM) and different CS-C18_33 mass fractions. Cur exhibited weak fluorescence in the aqueous phase, which increased after the transition to the hydrophobic domains formed by CS-C18_33 alkyl groups. The CAC value, determined from the dependence of Cur fluorescence intensity on the polymer content (**Fig. S3**), was 0.021 ± 0.004 mg/mL. This value is very close to that determined for CS-C18_33 in the absence of the drug, indicating that hydrophobic drugs have rather little impact on the aggregation of amphiphilic polysaccharides in an aqueous environment.

The ability of CS-C18_33 micelles to accumulate hydrophobic drugs was checked based on the encapsulation of Cur. Cur is expected to preferentially localize in the hydrophobic cores, as indicated by the high value of its lipophilicity parameter, log $P = 3.2$ (Kharat et al., 2017). First, we determined the so-called binding constant (K_b), which quantifies the partitioning of Cur between the polymer and water phases, and is defined as follows (Zatorska et al., 2020):

$$K_b = \frac{c_P}{c_w c_{CS-C18}} \tag{1}$$

where c_P and c_w are the concentrations of Cur in the polymer and water phases, respectively, and c_{CS-C18} is the concentration of CS-C18_33. Hence, the ratio of drug concentrations in the polymer and aqueous phases can be calculated as follows

$$\frac{c_P}{c_w} = K_b c_{CS-C18} \tag{2}$$

The penetration of Cur into the CS-C18_33 micelles was examined by measuring the fluorescence spectra of solutions containing a fixed Cur concentration and different polymer concentrations (Fig. 7A). As mentioned above, Cur shows weak emission in aqueous solution, so the increase in fluorescence intensity with increasing polymer concentration can be attributed to its partitioning into the hydrophobic domains of the polymer micelles. The K_b value is determined by fitting a line to the dependence of the maximum intensity of Cur emission on the CS-C18_33 concentration (Fig. 7B) according to the equation (Kępczyński & Ehrenberg, 2002):

$$F = \frac{F_{init} + F_{com} K_b c_{CS-C18}}{1 + K_b c_{CS-C18}} \tag{3}$$

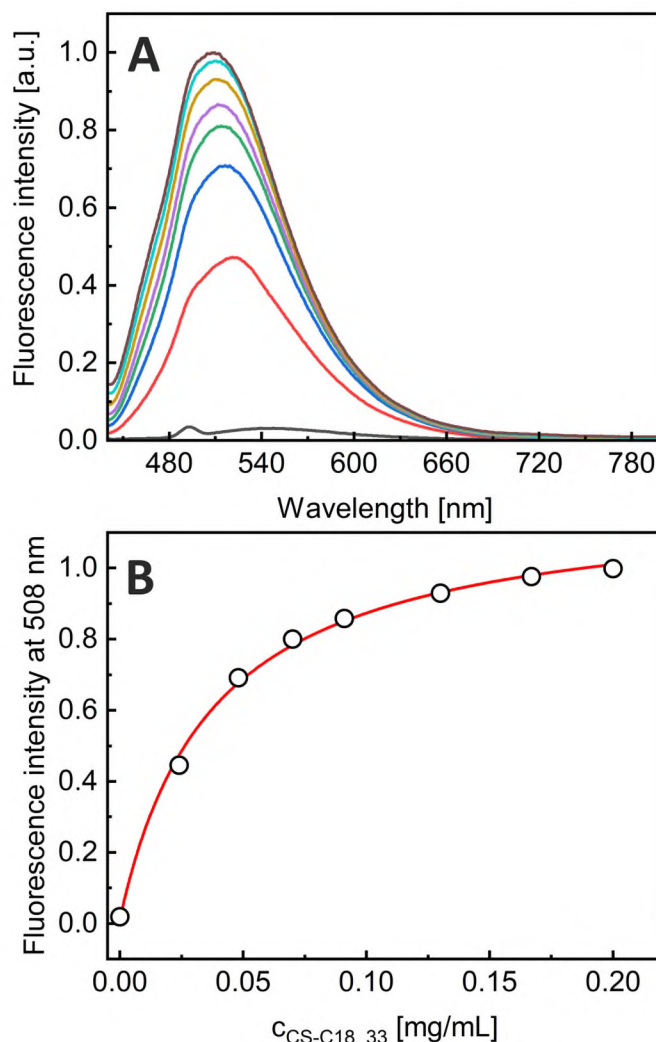where F_{init}, F, and F_{com} are the Cur emission intensities measured in the

Fig. 7. (A) Fluorescence spectra of Cur (0.7 μM, $\lambda_{exc} = 422$ nm) in the presence of different CS-C18_33 concentrations. (B) Emission intensity of Cur at 508 nm as a function of the CS-C18_33 concentration. The line fitted to eq. 2 is shown in red.

aqueous solution, in the presence of the polymer at a concentration of c_{CS-C18}, and at complete incorporation, respectively. The fitting revealed that the K_b value was equal to 26.5 ± 2.2 (mg/mL)$^{-1}$. Thus, at $c_{CS-C18} = 0.4$ mg/mL, the ratio of Cur concentrations in the polymer and water phases was about 10. In comparison, the K_b value for the penetration of Cur into amphiphilic block copolymer nanoparticles is about 10.4 (mg/mL)$^{-1}$ (Zatorska et al., 2020). This indicates that the affinity of Cur for the CS-C18_33 micelles is very high, so nanoparticles from amphiphilic CSs should be effective carriers of hydrophobic drugs.

Conventionally, the ability of a given DDS to accumulate drugs is quantified by two parameters: the drug loading capacity (DLC, defined as the ratio of the mass of drug entrapped in the polymer phase to the mass of polymer, Eq. S1) and the encapsulation efficiency (EE, defined as the ratio the mass of drug entrapped in the polymer phase to the mass of drug added initially during preparation, Eq. S2). We determined the DLC and EE values for the CS-C18_33 micelles for different initial Cur contents (**Table S3**). The DLC values indicate that the CS-C18_33 nanoparticles can accumulate up to 20 wt-% of Cur with relative to the polymer mass during micelle preparation. While the EE values show that these micelles can retain Cur up to 95 % of the drug introduced during their preparation. For comparison, DLC and EE of nanostructures prepared from amphiphilic copolymers were 11 to 13 wt-% and 26 to 37 wt-%, respectively (Zatorska et al., 2020; Zatorska-Plachta et al., 2021).

Recently, mixed chitosan/CS nanoparticles were shown to retain about 80 % of Cur (Jardim et al., 2020). Thus, the hydrophobically modified polysaccharides form nanoparticles with enhanced ability to accumulate hydrophobic drugs. In addition, the nanostructures obtained from amphiphilic polysaccharides have much better accumulation capacity for drugs compared to those from amphiphilic block copolymers.

4.7. The embedded Cur changes the morphology of the CS-C18 nanostructures

Finally, the effect of hydrophobic drug encapsulation on the morphology and molecular organization of the CS-C18 micelles was investigated. At the preparation step, 10 or 20 wt% Cur relative to the mass of the polymer was incorporated into the CS-C18_33 nanoparticles. The size of Cur-loaded nanoparticles was much larger than the empty CS-C18_33 micelles (Table 1), but the introduction of the drug did not change the zeta potential, which shows that Cur penetrates the hydrophobic core. The morphology of the Cur-loaded particles was observed using cryo-TEM. Typical micrographs are shown in **Fig. 3**E and **F**. The most abundant objects were irregular structures with sizes of 30–510 nm. Small grains with higher contrast distributed almost uniformly inside the CS-C18_33 nanoparticles can be easily observed. The appearance of these grains was attributed to the formation of curcumin nanoaggregates during preparation. Small globular micelles that built larger clusters of irregular shape were also present in the dispersion (Fig. 3F). In this case, the small grains with higher contrast were also embedded within the clusters.

To better understand how the incorporation of a hydrophobic drug affects the molecular organization of the CS-C18 nanoparticles and how the drug is the spatially distributed within these structures, we simulated systems containing four CS-C18$_{100}$ oligomers and 18 Cur molecules (system **G**), corresponding to a drug content of 15 wt% relative to the polymer mass. A snapshot showing the final configuration of the system is shown in Fig. 6B. In the presence of Cur, the oligomers self-organized into a multi-core micelle of irregular shape. All the drug molecules were entrapped in the resulting micelle, confirming the high affinity of Cur for CS-C18 nanoparticles. The two-dimensional mass density map across the Cur-loaded CS-C18$_{100}$ nanoparticles was calculated (Fig. 6). As can be seen, Cur is not evenly distributed in the hydrophobic cores. The center of the cores remains empty, and the drug molecules preferentially locate at the interface between the hydrophobic part and the hydrophilic corona formed by the hydrated CS chains. We calculated the number of contacts between Cur and CS chains and Cur and C18 groups averaged over the last 120 ns (**Table S2**). The numbers of contacts show that the drug molecules are mostly surrounded by the octadecyl groups, but partially interact with the polysaccharide chain.

The strong interaction of Cur with the octadecyl groups should affect the interactions between these groups within the CS-C18 nanostructures. Both microscopic observations and simulations showed a large influence of the presence of Cur on the morphology of the micelles formed. To confirm that Cur can alter interactions within micelles, the intermolecular and intramolecular contacts between hydrophobic groups were estimated (**Table S1**). Comparison of systems **B2** (without the drug) and **G** (with Cur embedded) systems shows that the incorporation of Cur significantly reduced the total number of interactions between C18 groups, mainly due to a decrease in the intermolecular interactions. In contrast, an increase in N_{intra} was observed. Thus, encapsulation of Cur in CS-C18 nanoparticles significantly disrupts the interactions between hydrophobic groups attached to the main polysaccharide chain, changing their nature from intermolecular to more intramolecular, which affects the morphology of the resulting Cur-loaded micelles.

5. Conclusions

In this work, we discussed how the degree of CS backbone grafting

with hydrophobic groups affects the ability of polysaccharide chains to self-organize in aqueous environments. It should be emphasized that such amphiphilic derivatives are non-homogeneous polymeric materials. The chains differ in length, degree of substitution, and distribution of hydrophobic groups along a given CS chain, which significantly affect their behavior in aqueous media. In addition, the attachment of hydrophobic groups has a moderate effect on the hydration of CS chains and amphiphilic CS derivatives remain highly hydrated in aqueous dispersions.

Our study demonstrated a strong influence of DS and the polymer concentration on the self-organization of amphiphilic CSs and the morphology of the aggregates. For low DS, mainly irregular, highly hydrated nanogels were observed. Increasing the degree of grafting with hydrophobic groups led to the formation of cylindrical micelles. While amphiphilic CSs with high DS preferentially formed large cylindrical micelles or spherical monomolecular micelles, depending on the polymer concentration, both with a core-shell structure. The microscopic observations showed that nanogels and cylindrical micelles can coexist with each other in equilibrium. The existence in equilibrium of structures with different morphologies indicates segregation in the aggregation of polymer chains differing in substitution with hydrophobic groups. In a given system, polymer chains with lower alkyl substitution form loosely packed structures, while chains with higher hydrophobic substitution aggregate separately to form more compact cylindrical micelles. Our simulations show that the degree of CS substitution affect the intermolecular and intramolecular interactions between alkyl groups, and thus influences the morphology of the aggregates. At low DS, polysaccharide chains adopt elongated conformations. The low density of hydrophobic groups along the CS chain results in negligible intramolecular interactions, so such derivatives can aggregate due to interactions between hydrophobic groups attached to different chains. Increasing the number of hydrophobic substituents increases the possibility of intramolecular interactions, which leads to the formation of hydrophobic domains, as a result, the polysaccharide chains become more coiled and the whole structure is better defined, forming nanogels. The size of the hydrophobic domains should increase with increasing DS. Increasing the density of alkyl groups along the chain enhances intramolecular interactions, which promotes the formation of hydrophobic cores. Beyond a certain content of alkyl groups, well-defined densely packed structures are formed, the morphology of which depends on the polymer concentration. At concentrations below CAC, monomolecular micelles can form as a result of intramolecular contacts, which can assemble into larger clusters. In contrast, above CAC, elongated multicore micelles predominate, whose structure is stabilized by intermolecular contacts between hydrophobic groups. The alkyl groups formed densely packed hydrophobic cores that were surrounded by well-hydrated CS chains.

An important outcome of our study is that nanoparticles prepared from CS-C18 with high DS can effectively accumulate hydrophobic drugs. However, the Cur example shows that drug molecules are not evenly distributed in the hydrophobic cores and can preferentially locate at the interface between the hydrophobic part and the hydrophilic corona formed by the hydrated CS chains. In addition, the presence of Cur significantly affects the interactions between the hydrophobic groups attached to the polysaccharide chain, resulting in changes in the morphology of the Cur-loaded CS-C18 nanostructures.

The present results indicate that a combined approach using comprehensive experimental and computer simulation methods is adequate for understanding the behavior of amphiphilic polysaccharides in the aqueous media. Further studies should include polysaccharides grafted with hydrophilic groups of various structures.

CRediT authorship contribution statement

Agata Żak: Investigation, Methodology, Writing – original draft. **Grzegorz Łazarski:** Investigation, Methodology, Visualization, Writing

– original draft. **Magdalena Wytrwal-Sarna:** Investigation. **Dorota Jamróz:** Methodology, Writing – original draft. **Magdalena Górniewicz:** Investigation. **Aleksander Foryś:** Investigation. **Barbara Trzebicka:** Formal analysis, Methodology, Writing – original draft. **Mariusz Kepczynski:** Conceptualization, Project administration, Supervision, Funding acquisition, Writing - original draft, Writing - review & editing.

Declaration of competing interest

The authors declare that they have no known competing financial interests or personal relationships that could have appeared to influence the work reported in this paper.

Data availability

Molecular insights into the self-assembly of hydrophobically modified chondroitin sulfate in aqueous media - Additional Data (Original data) (Mendeley Data)

Acknowledgments

Appendix A. Supplementary data

Supplementary data to this article can be found online at https://doi.org/10.1016/j.carbpol.2022.119999.

References

Abraham, M. J., Murtola, T., Schulz, R., Páll, S., Smith, J. C., Hess, B., & Lindah, E. (2015). GROMACS: High performance molecular simulations through multi-level parallelism from laptops to supercomputers. *SoftwareX, 1–2,* 19–25.

Allen, T. M., & Cullis, P. R. (2004). Drug delivery systems: Entering the mainstream. *Science, 303*(5665), 1818–1822.

Amhare, A. F., Lei, J., Deng, H., Lv, Y., Han, J., & Zhang, L. (2020). Biomedical application of chondroitin sulfate with nanoparticles in drug delivery systems: Systematic review. *Journal of Drug Targeting, 29*(3), 259–268.

Anjomshoa, S., Namazian, M., & Noorbala, M. R. (2016). The effect of solvent on tautomerism, acidity and radical stability of curcumin and its derivatives based on thermodynamic quantities. *Journal of Solution Chemistry, 45*(7), 1021–1030.

Cadete, A., Olivera, A., Besev, M., Dhal, P. K., Gonçalves, L., Almeida, A. J., Bastiat, G., Benoit, J. P., de la Fuente, M., Garcia-Fuentes, M., Alonso, M. J., & Torres, D. (2019). Self-assembled hyaluronan nanocapsules for the intracellular delivery of anticancer drugs. *Scientific Reports, 9*(1), 11565.

Cellet, T. S. P., Pereira, G. M., Muniz, E. C., Silva, R., & Rubira, A. F. (2015). Hydroxyapatite nanowhiskers embedded in chondroitin sulfate microspheres as colon targeted drug delivery systems. *Journal of Materials Chemistry B, 3*(33), 6837–6846.

Chattopadhyay, A., & London, E. (1984). Fluorimetric determination of critical micelle concentration avoiding interference from detergent charge. *Analytical Biochemistry, 139*(2), 408–412.

Darden, T., York, D., & Pedersen, L. (1998). Particle mesh Ewald: An N·log(N) method for Ewald sums in large systems. *The Journal of Chemical Physics, 98*(12), 10089.

Hess, B., Bekker, H., Berendsen, H. J. C., & Fraaije, J. G. E. M. (1997). LINCS: A linear constraint solver for molecular simulations. *Journal of Computational Chemistry, 18,* 1463–1472.

Humphrey, W., Dalke, A., & Schulten, K. (1996). VMD: Visual molecular dynamics. *Journal of Molecular Graphics, 14*(1), 33–38.

Hunter, J. D. (2007). Matplotlib: A 2D graphics environment. *Computing in Science and Engineering, 9*(3), 90–95.

Jardim, K. V., Siqueira, J. L. N., Báo, S. N., Sousa, M. H., & Parize, A. L. (2020). The role of the lecithin addition in the properties and cytotoxic activity of chitosan and chondroitin sulfate nanoparticles containing curcumin. *Carbohydrate Polymers, 227,* Article 115351.

Jo, S., Kim, T., Iyer, V. G., & Im, W. (2008). CHARMM-GUI: A web-based graphical user interface for CHARMM. *Journal of Computational Chemistry, 29*(11), 1859–1865.

Jorgensen, W. L., Chandrasekhar, J., Madura, J. D., Impey, R. W., & Klein, M. L. (1998). Comparison of simple potential functions for simulating liquid water. *The Journal of Chemical Physics, 79*(2), 926.

Karewicz, A., Bielska, D., Gzyl-Malcher, B., Kepczynski, M., Lach, R., & Nowakowska, M. (2011). Interaction of curcumin with lipid monolayers and liposomal bilayers. *Colloids and Surfaces B: Biointerfaces, 88*(1), 231–239.

Kaufmann, J., Möhle, K., Hofmann, H. J., & Arnold, K. (1999). Molecular dynamics of a tetrasaccharide subunit of chondroitin 4-sulfate in water. *Carbohydrate Research, 318* (1–4), 1–9.

Kępczyński, M., & Ehrenberg, B. (2002). Interaction of dicarboxylic metalloporphyrins with liposomes. The effect of pH on membrane binding revisited. *Photochemistry and Photobiology, 76*(5), 486–492.

Kepczynski, M., & Jamróz, D. (2020). Curcumin parametrization in the CHARMM force field. *Mendeley Data, v1.* 10.17632/mb9vy67sff.1.

Kępczyński, M., Nawalany, K., Jachimska, B., Romek, M., & Nowakowska, M. (2006). Pegylated tetraarylporphyrin entrapped in liposomal membranes: A possible novel drug-carrier system for photodynamic therapy. *Colloids and Surfaces B: Biointerfaces, 49*(1), 22–30.

Khan, A. R., Liu, Y., Yang, H., Yang, X., Liu, S., Ji, J., & Zhai, G. (2020). Chondroitin sulfate-based redox-responsive nanoparticles for melanoma-targeted drug delivery. *Journal of Drug Delivery Science and Technology, 60,* Article 102033.

Kharat, M., Du, Z., Zhang, G., & McClements, D. J. (2017). Physical and chemical stability of curcumin in aqueous solutions and emulsions: Impact of pH, temperature, and molecular environment. *Journal of Agricultural and Food Chemistry, 65*(8), 1525–1532.

King, E., Qi, R., Li, H., Luo, R., & Aitchison, E. (2021). Estimating the roles of protonation and electronic polarization in absolute binding affinity simulations. *Journal of Chemical Theory and Computation, 17*(4), 2541–2555.

Kowalczuk, A., Trzcinska, R., Trzebicka, B., Müller, A. H. E., Dworak, A., & Tsvetanov, C. B. (2014). Loading of polymer nanocarriers: Factors, mechanisms and applications. *Progress in Polymer Science, 39*(1), 43–86.

Lee, J., Cheng, X., Swails, J. M., Yeom, M. S., Eastman, P. K., Lemkul, J. A., Wei, S., Buckner, J., Jeong, J. C., Qi, Y., Jo, S., Pande, V. S., Case, D. A., Brooks, C. L., MacKerell, A. D., Klauda, J. B., & Im, W. (2016). CHARMM-GUI input generator for NAMD, GROMACS, AMBER, OpenMM, and CHARMM/OpenMM simulations using the CHARMM36 additive force field. *Journal of Chemical Theory and Computation, 12* (1), 405–413.

Lewandowska, J., Kępczyński, M., Bednar, J., Rząd, E., Moravcikova, V., Jachimska, B., & Nowakowska, M. (2009). Silicone-stabilized liposomes. *Colloid and Polymer Science, 288*(1), 37–45.

Li, L., Raghupathi, K., Song, C., Prasad, P., & Thayumanavan, S. (2014). Self-assembly of random copolymers. *Chemical Communications, 50*(88), 13417–13432.

Li, M., Sun, J., Zhang, W., Zhao, Y., Zhang, S., & Zhang, S. (2021). Drug delivery systems based on CD44-targeted glycosaminoglycans for cancer therapy. *Carbohydrate Polymers, 251,* Article 117103.

Liang, Y., Fu, X., Du, C., Xia, H., Lai, Y., & Sun, Y. (2020). Enzyme/pH-triggered anticancer drug delivery of chondroitin sulfate modified doxorubicin nanocrystal. *Artificial Cells, Nanomedicine and Biotechnology, 48*(1), 1114–1124.

Liu, M., Du, H., & Zhai, G. (2016). Self-assembled nanoparticles based on chondroitin sulfate-deoxycholic acid conjugates for docetaxel delivery: Effect of degree of substitution of deoxycholic acid. *Colloids and Surfaces B: Biointerfaces, 146,* 235–244.

Liu, M., Du, H., Khan, A. R., Ji, J., Yu, A., & Zhai, G. (2018). Redox/enzyme sensitive chondroitin sulfate-based self-assembled nanoparticles loading docetaxel for the inhibition of metastasis and growth of melanoma. *Carbohydrate Polymers, 184,* 82–93.

Liu, Z., Zhang, Z., Zhou, C., & Jiao, Y. (2010). Hydrophobic modifications of cationic polymers for gene delivery. *Progress in Polymer Science, 35*(9), 1144–1162.

Misra, S., Hascall, V. C., Atanelishvili, I., Moreno Rodriguez, R., Markwald, R. R., & Ghatak, S. (2015). Utilization of glycosaminoglycans/proteoglycans as carriers for targeted therapy delivery. *International Journal of Cell Biology, 2015,* 1–25.

Oommen, O. P., Duehrkop, C., Nilsson, B., Hilborn, J., & Varghese, O. P. (2016). Multifunctional hyaluronic acid and chondroitin sulfate nanoparticles: Impact of glycosaminoglycan presentation on receptor mediated cellular uptake and immune activation. *ACS Applied Materials and Interfaces, 8*(32), 20614–20622.

Park, S. J., Lee, J., Qi, Y., Kern, N. R., Lee, H. S., Jo, S., Joung, I., Joo, K., Lee, J., & Im, W. (2019). CHARMM-GUI glycan modeler for modeling and simulation of carbohydrates and glycoconjugates. *Glycobiology, 29*(4), 320–331.

Park, W., Park, S.j., & Na, K. (2010). Potential of self-organizing nanogel with acetylated chondroitin sulfate as an anti-cancer drug carrier. *Colloids and Surfaces B: Biointerfaces, 79*(2), 501–508.

Parrinello, M., & Rahman, A. (1998). Polymorphic transitions in single crystals: A new molecular dynamics method. *Journal of Applied Physics, 52*(12), 7182.

Pippa, N., Gazouli, M., & Pispas, S. (2021). Recent advances and future perspectives in polymer-based nanovaccines. *Vaccines, 9,* 558.

Pronk, S., Páll, S., Schulz, R., Larsson, P., Bjelkmar, P., Apostolov, R., Shirts, M. R., Smith, J. C., Kasson, P. M., van der Spoel, D., Hess, B., & Lindahl, E. (2013). GROMACS 4.5: A high-throughput and highly parallel open source molecular simulation toolkit. *Bioinformatics, 29*(7), 845–854.

Servaty, R., Schiller, J., Binder, H., & Arnold, K. (2001). Hydration of polymeric components of cartilage — An infrared spectroscopic study on hyaluronic acid and chondroitin sulfate. *International Journal of Biological Macromolecules, 28*(2), 121–127.

van der Spoel, D., Lindahl, E., Hess, B., Groenhof, G., Mark, A. E., & Berendsen, H. J. C. (2005). GROMACS: Fast, flexible, and free. *Journal of Computational Chemistry, 26* (16), 1701–1718.

Szafraniec, J., Błazejczyk, A., Kus, E., Janik, M., Zajac, G., Wietrzyk, J., Chlopicki, S., & Zapotoczny, S. (2017). Robust oil-core nanocapsules with hyaluronate-based shells as promising nanovehicles for lipophilic compounds. *Nanoscale, 9*(47), 18867–18880.

Václavíková, E., & Kvasnička, F. (2015). Quality control of chondroitin sulphate used in dietary supplements. *Czech Journal of Food Sciences, 33*, 165–173.

Wytrwal, M., Sarna, M., Bednar, J., Kozik, B., Nowakowska, M., & Kepczyński, M. (2011). Formation of micelles by hydrophobically modified poly(allylamine hydrochloride). *Polish Journal of Applied Chemistry, 55*, 11–17.

Xiao, Y., Li, P., Cheng, Y., Zhang, X., Sheng, J., Wang, D., Li, J., Zhang, Q., Zhong, C., Cao, R., & Wang, F. (2014). Enhancing the intestinal absorption of low molecular weight chondroitin sulfate by conjugation with α-linolenic acid and the transport mechanism of the conjugates. *International Journal of Pharmaceutics, 465*(1–2), 143–158.

Xie, X., Yuan, Z., Yuan, Q., Huang, Y., Yu, Q., Ren, J., Liang, L., Jin, H., & Yu, J. (2021). Preparation and characterization of amphiphilic nanoparticles based on chondroitin sulfate a conjugated with hydrophobic drug for enhanced doxorubicin delivery. *Colloid and Polymer Science, 299*(1), 129–136.

Yang, J., Shen, M., Wen, H., Luo, Y., Huang, R., Rong, L., & Xie, J. (2020). Recent advance in delivery system and tissue engineering applications of chondroitin sulfate. *Carbohydrate Polymers, 230*, Article 115650.

Yang, X., Shi, X., D'arcy, R., Tirelli, N., & Zhai, G. (2018). Amphiphilic polysaccharides as building blocks for self-assembled nanosystems: Molecular design and application in cancer and inflammatory diseases. *Journal of Controlled Release, 272*, 114–144.

Zatorska, M., Łazarski, G., Maziarz, U., Wilkosz, N., Honda, T., Yusa, S.i., … Kepczynski, M. (2020). Drug-loading capacity of polylactide-based micro- and nanoparticles – Experimental and molecular modeling study. *International Journal of Pharmaceutics, 591*, Article 120031.

Zatorska-Płachta, M., Łazarski, G., Maziarz, U., Foryś, A., Trzebicka, B., Wnuk, D., Chołuj, K., Karewicz, A., Michalik, M., Jamroz, D., & Kepczynski, M. (2021). Encapsulation of curcumin in polystyrene-based nanoparticles-drug loading capacity and cytotoxicity. *ACS Omega, 6*(18), 12168–12178.

Zhao, L., Liu, M., Wang, J., & Zhai, G. (2015). Chondroitin sulfate-based nanocarriers for drug/gene delivery. *Carbohydrate Polymers, 133*, 391–399.